

# Universal manuscript template for Optica Publishing Group journals

## 1. Abstract

2 Lorem ipsum ~100 words

## 3 2. Introduction

4 IR spectroscopy has seen significant interest and application in bio-imaging because it provides a  
5 chemical fingerprint of underlying samples in a label-free way [1]. However, although the most  
6 relevant chemical information can be gathered in the mid-infrared ( $\sim 3 - 12 \mu\text{m}$ ), slow signal  
7 acquisition is often a limiting factor, whose trade-off can keep it from competing with label-based  
8 fluorescence microscopy.

9 Fig. 1 attempts to visualize the significant developments that have been made in mid-infrared  
10 hyperspectral imaging over roughly the last two decades. Experiments are mapped onto the  
11 two important metrics of spectra acquisition speed, which captures the rate at which spectra  
12 are gathered, and optical bandwidth, which captures the breadth of chemical content that can  
13 be observed. The two variables are plotted against each other, since a significant difficulty lies  
14 in achieving both metrics simultaneously. For a better one to one comparison, the acquisition  
15 speeds listed for experiments that use focal plane arrays have been normalized to that of an  
16 analogous point scanning experiment.  
17

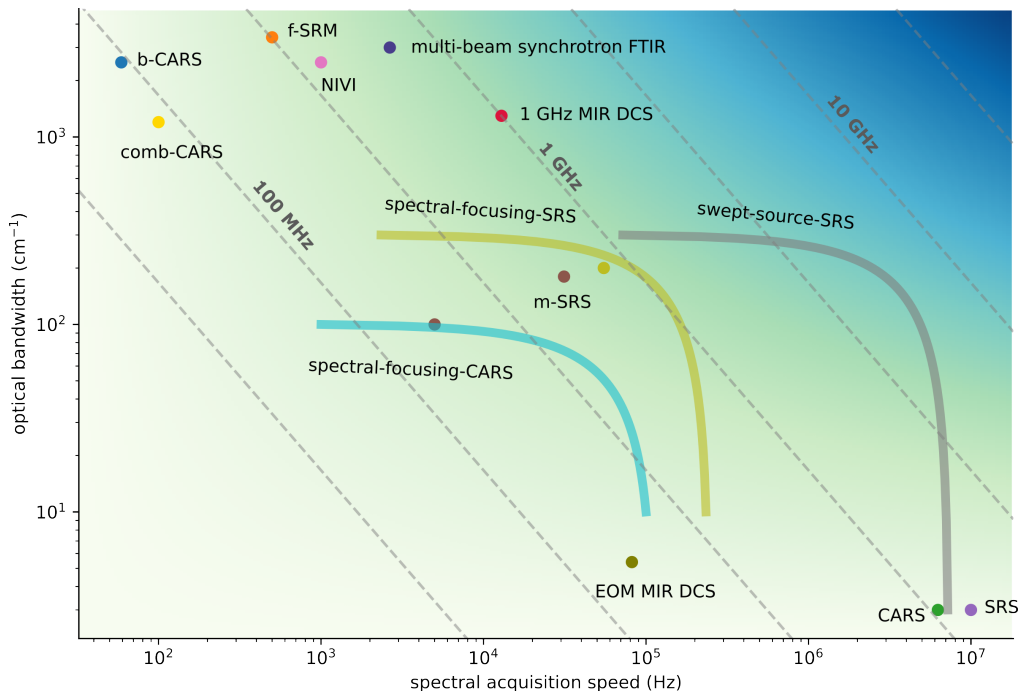


Fig. 1. Performance map of mid-infrared hyperspectral imaging. Broadband CARS (b-CARS) [2], femtosecond Stimulated Raman Microscopy (f-SRM) [3], in-vivo video rate CARS [4], in-vivo video rate SRS [5], multiplexed SRS (m-SRS) [6, 7], nonlinear interferometric vibrational imaging (NIVI) [8], swept-source SRS [9], spectral-focusing SRS [10], spectral-focusing CARS [11], spectral-focusing SRS [12], comb-CARS [13], multi-beam synchrotron FTIR [14], electro-optic modulator comb MIR DCS [15]

19 A few of the most notable experiments have utilized coherent Raman spectro-imaging, where  
 20 in-vivo video-rate speeds have been demonstrated in the mid-infrared [4, 5]. Whereas initial  
 21 demonstrations were over a narrow bandwidth ( $\sim 3 \text{ cm}^{-1}$ ), broad bandwidths at high acquisition  
 22 speeds have been demonstrated using rapidly rotating polygonal mirror scanners [12, 16]. However,  
 23 the stated metrics are only possible with the strong Raman absorption cross-sections around  
 24  $2900 \text{ cm}^{-1}$ , which precludes Raman spectroscopy-based platforms from achieving the same  
 25 performance in the fingerprint region at longer wavelengths.

26 Conversely, Fourier transform spectroscopy (FTS) and quantum cascade laser (QCL) based  
 27 imaging are attractive due to their broad applicability across the mid to long wavelength infrared.  
 28 The high absorption cross-sections can also alleviate the need for operation at powers close to  
 29 sample-damage thresholds, a concern that is applicable to biological samples. In this category,  
 30 FTS spectrometers coupled to broadband and bright sources such as synchrotron facilities have  
 31 set the state of the art for the combination of spectral bandwidth and speed [14]. The coupling of  
 32 broadband synchrotron light into a microscope requires the active stabilization of a beam bundle.  
 33 However, a widely accessible imaging method would benefit from having a simple and table  
 34 top setup. QCL lasers are attractive due to their direct emission in the mid-infrared and small  
 35 footprint, although their performance is best leveraged in narrowband applications. Tunable QCL  
 36 packages consisting of multiple QCL chips combined into one device [17] can nominally reach  
 37 broad spectral coverage, but struggle to reach noise figures comparable to platforms based on  
 38 mode-locked lasers.

More recently, dual-comb spectroscopy (DCS) in the frequency comb community has become  
 a popular platform, due to its improved stability and speed when compared to classical FTS [18].  
 In this modality, the interference of two frequency combs maps a Nyquist band from the optical  
 domain down into the RF. One of the most important considerations in DCS is the direct trade-off  
 between the frequency resolution/repetition rate  $f_r$  and the size of the optical Nyquist window  
 $\Delta\nu$ :

$$\Delta\nu = \frac{f_r^2}{2\Delta f_r} \quad (1)$$

39 where  $\Delta f_r$  is the interferogram acquisition rate equal to the difference of the two laser rep-rates.  
 40 The diagonal dashed lines in Fig. 1., show the  $f_r^2/2$  trade-off between resolvable bandwidth and  
 41 acquisition speed in DCS for different  $f_r$ . Evidently, when broad absorption features allow for  
 42 coarse resolution, the highest rep-rates are desired. However, in order to reach sufficient power  
 43 per comb tooth, in practice the pulse energy required for nonlinear frequency down-conversion  
 44 from the near-infrared sets an upper limit on the obtainable rep-rate. In this work, we utilize a  
 45 set of recently developed 1-GHz mid-infrared frequency combs [19] to integrate a dual-comb  
 46 spectrometer with a confocal microscope. We capitalize on the high repetition rate by fully filling  
 47 the third Nyquist band ( $2595 \text{ cm}^{-1}$ – $3890 \text{ cm}^{-1}$  at  $\Delta f_r = 12.86 \text{ kHz}$ ). The system is among the  
 48 fastest performers in the class of spectrometers covering over  $1000 \text{ cm}^{-1}$  with high spectral  
 49 resolution in the mid-infrared.

50 However, pointing to the dashed line in the upper right corner of Fig. 1, in order to achieve the  
 51 ultimate goal of label-free broadband video-rate imaging, we note that the ideal DCS platform  
 52 would operate with repetition rates of 10 GHz or higher. Such systems would likely require either  
 53 high-power amplifiers or a nanophotonic design capable of generating equivalent bandwidths in  
 54 the mid-infrared with pump pulse energies around 100 pJ.

### 55 3. Experiment

56 With long-term stability in mind, a single-branch intra-pulse difference frequency generation  
 57 (DFG) design is used to generate light in the mid-infrared [19]. Shown in Fig. 2, to compensate  
 58 for the low conversion efficiency of the single-branch design, octave spanning few cycle NIR

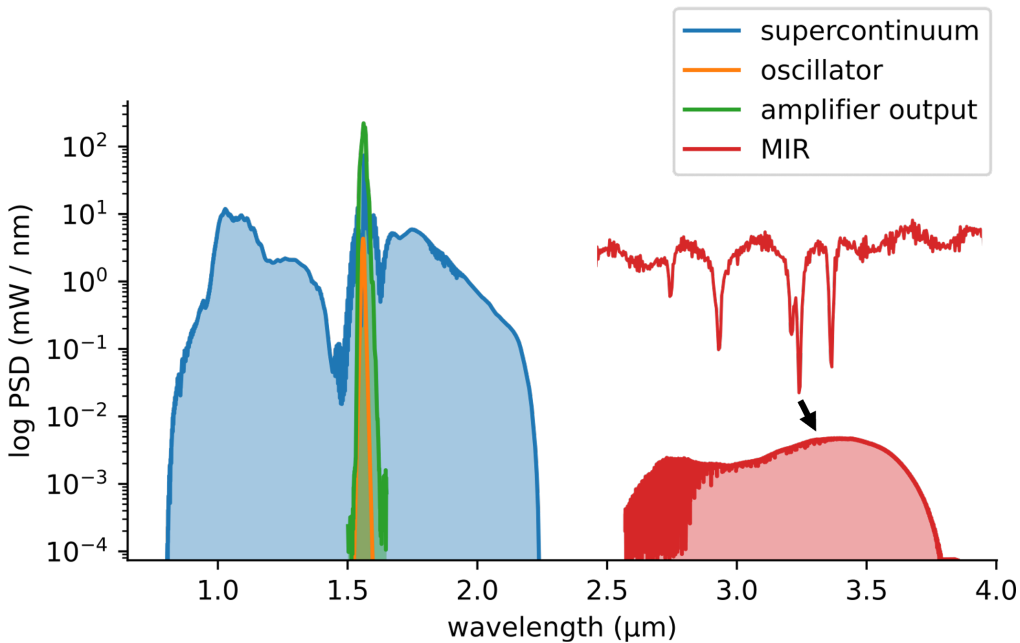


Fig. 2. 1 GHz MIR Frequency Comb. The spectral evolution through successive stages of the system: oscillator → chirped-pulse amplifier → few-cycle supercontinuum generation → MIR frequency down conversion. The inset shows a zoom in of waterlines that are resolved when using the full 1 GHz frequency resolution.

59 pulses generated via soliton self-compression in anomalous dispersion highly nonlinear fiber are  
 60 used to drive the nonlinear frequency down conversion to the mid-infrared. Although coverage  
 61 of the 6-12  $\mu\text{m}$  wavelength region can be achieved for one laser system, due to the lack of  
 62 nonlinear crystals in this work more widely available lithium niobate is used to cover the 3 - 5  
 63  $\mu\text{m}$  wavelength window.

64 Two 1-GHz mid-infrared frequency combs are generated and coupled into  $\text{InF}_3$  single-mode  
 65 fiber for delivery to the experiment. The output beam is collimated with a two inch off-axis  
 66 parabolic mirror, and a reflective confocal microscope with 0.58 NA is used to image the beam  
 67 onto a glass slide ( $\sim 3.8 \mu\text{m}$  pixel size). A set of linear translation stages are used to raster scan  
 68 the sample. The data is acquired via trigger, with the trigger spacing and scan speed set by the  
 69 desired spatial sampling interval. The scan speed is limited only by the interferogram acquisition  
 70 time, which is fundamentally set by the repetition rate of the laser. The transmitted signal is  
 71 focused onto a high-speed MCT detector, whose AC coupled port is digitized at 1 GS/s using an  
 72 FPGA (GaGe model #). The data is streamed concurrently from the card memory into PC RAM  
 73 for real-time analysis, and such that the card-memory does not limit the data volume. Owing to  
 74 the fairly high 500 MHz Nyquist frequency [20, 21], and the placement of all fiber amplifiers in  
 75 loop for the phase-locks of the two frequency combs, over one thousand interferograms can be  
 76 directly averaged before phase correction needs to be employed.

#### 77 4. Results

78 As a demonstration, hyperspectral images are taken of a USAF resolution target composed of  
 79 SU-8 photoresist patterned onto a 500  $\mu\text{m}$  thick Silicon wafer. Five hundred spectra (39 ms) are  
 80 averaged at each pixel and apodized to 100 GHz ( $3.3 \text{ cm}^{-1}$ ). Point spectra shown in Fig. 4.(b).  
 81 are taken at each pixel to generate the hypercube. The images are generated by integrating a

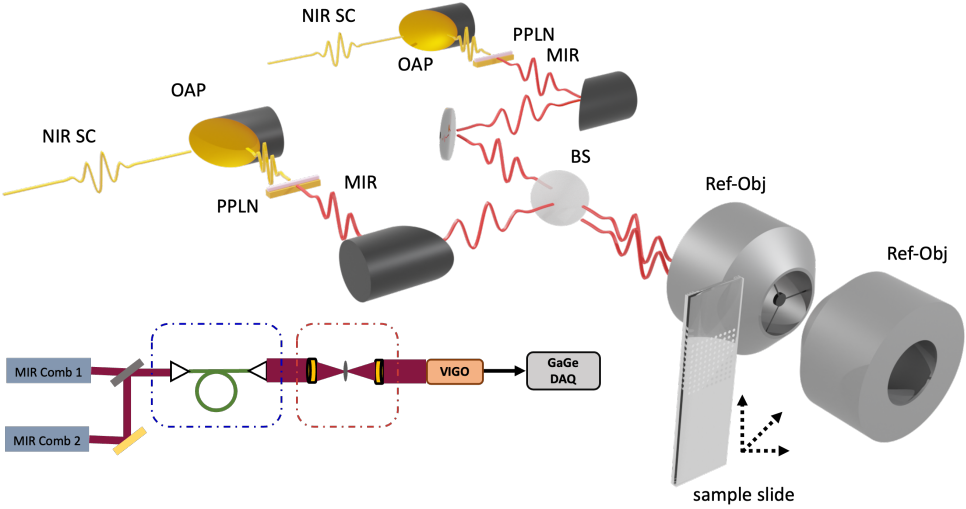


Fig. 3. Experimental Setup. Two mid-infrared frequency combs generated through intra-pulse difference frequency generation are passed collinearly through a confocal microscope. Hyperspectral images are collected by raster scanning the sample slide. The transmitted signal is collected and digitized in a high-speed MCT mid-infrared detector and FPGA.

82 ~63 cm<sup>-1</sup> window around the peak absorption at ~2930 cm<sup>-1</sup>.

83 For a biologically relevant sample, we image a cross-section of ovarian cancer tissue (... add  
 84 info), where the paraffin wax was removed prior to dual-comb imaging. To validate these results,  
 85 we compare the results of DCS point scanning microscopy to hyperspectral data taken with a  
 86 commercial FTIR microscope using a focal plane array (... add info). Five hundred spectra are  
 87 again averaged at each pixel and apodized to 3.3 cm<sup>-1</sup>. Point spectra such as the one shown  
 88 by the orange curve in Fig. 5.(b). are collected at each pixel, with the two C-H anti-symmetric  
 89 stretch bands visible at 2850 and 2920 cm<sup>-1</sup>. A DCS spectrum taken with a two second averaging  
 90 time (25,700 averages) is shown by the green curve, and a comparison spectrum taken using a  
 91 commercial FTIR with 7.61 cm<sup>-1</sup> frequency resolution is shown by the red curve. Apart from  
 92 a broadening of the peak, good agreement is observed between the DCS and FTIR spectra.  
 93 The FTIR image was taken prior to the removal of paraffin wax, which accounts for the peak  
 94 broadening when compared to the spectra taken using DCS. The images are generated by taking  
 95 a slice through the hypercube at the peak of the 2920 cm<sup>-1</sup> band. A coarse image shown in  
 96 Fig. 5.(c). with 5 μm sampling is taken of the entire core. A zoom-in of the sample is shown  
 97 in Fig. 5.(a)., taken at 1.2 μm sampling, which is approximately the Nyquist sampling limit of  
 98 the microscope. The image shows generally good agreement with the corresponding image in  
 99 Fig. 5.(d). taken using FTIR. We note that the dim vertical line scans in the DCS image are  
 100 attributed to the limited ~1.5 μm repeatability of the translation stages (Thorlabs Z825B).

## 101 5. Discussion

Regardless of the imaging method, the final determination of imaging speed is given by the time needed to reach sufficient SNR at each pixel. Specifically for DCS microscopy, the target SNR and frequency resolution sets the pixel dwell time. In DCS, the absorbance noise  $\sigma$  scales with

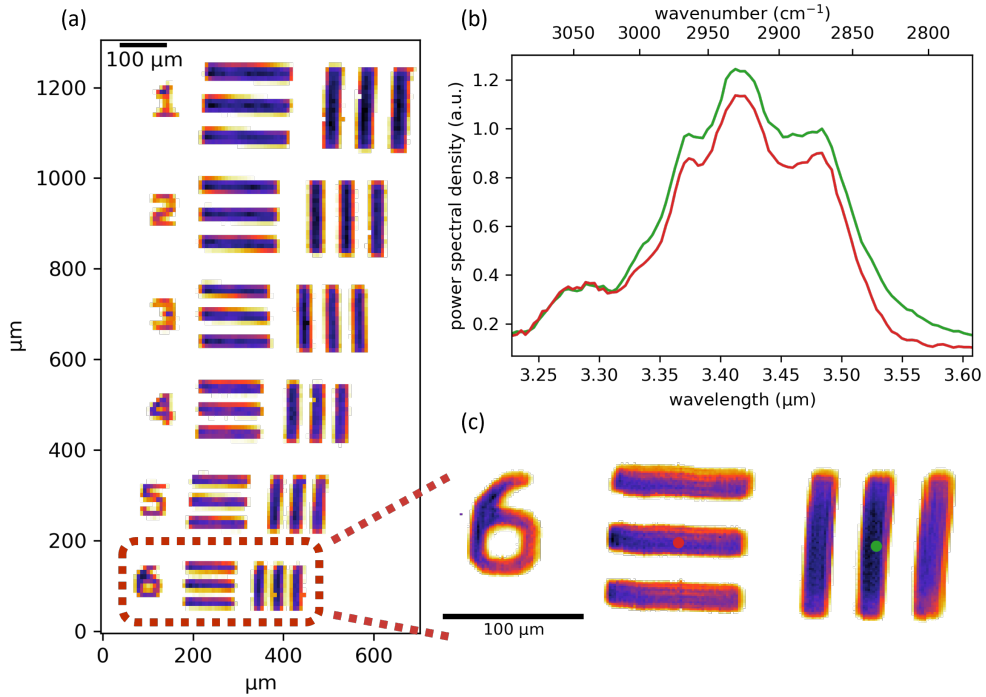


Fig. 4. Caption

the frequency resolution and number of averaged spectra  $N_{avg}$  according to [22]:

$$\sigma \propto \frac{N}{\sqrt{N_{avg}}} \quad (2)$$

where  $N$  is the number of frequency bins. This scaling rule is shown in Fig. 6.(c-d)., where it is observed to match the experimentally measured absorbance noise.

Shown in Fig. 6.(a)., a baseline for 1 GHz DCS is that a  $1000 \text{ cm}^{-1}$  Nyquist window can be covered with  $\sim 17$  kHz spectra acquisition speed. In Fig. 6.(b)., a single-shot spectrum ( $77 \mu\text{s}$ ) at 1 GHz resolution has low signal to noise, but can be averaged to high SNR in two seconds ( $>25,000$  spectra). However, a high SNR can be achieved in  $\sim 39$  ms at 500 averages if the interferograms are apodized to 100 GHz ( $\sim 3.33 \text{ cm}^{-1}$ ), which is a more appropriate sampling interval for the given absorption features.. The SNR as a function of averaging time and frequency resolution is shown in Fig. 6.(c-d).; the absorbance noise always averages down according to  $1/\sqrt{N_{avg}}$ , but with coarser resolution resulting in a directly proportional overall noise reduction.

All time scales change with the repetition rate as  $\propto 1/f_r^2$ . Consequently, the two-variable map in Fig. 6.(d). should apply more generally to DCS point scanning microscopy with lower and higher  $f_r$ , but with the time-axis scaled accordingly. As an example, well established 100 MHz mid-infrared DCS [23, 24] would reach the same SNR at 3.9 s per pixel extending the overall experiment time to over a day, [25], while 10 GHz DCS would reach the SNR in  $390 \mu\text{s}$  reducing the overall experiment time from hours to minutes.

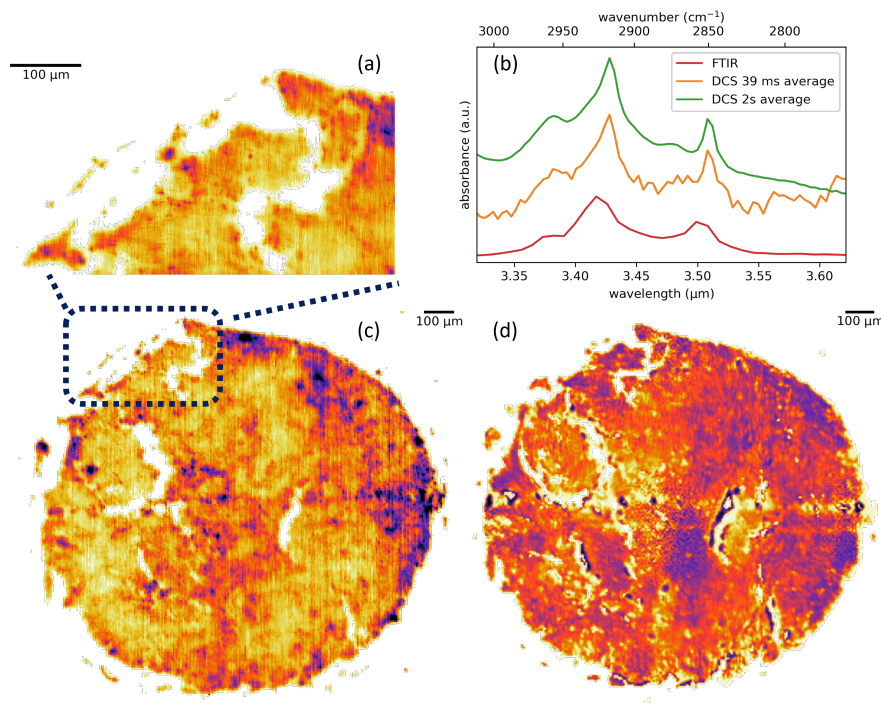


Fig. 5. Caption

## 118 6. Conclusion

### 119 References

- 120 1. M. J. Baker, J. Trevisan, P. Bassan, R. Bhargava, H. J. Butler, K. M. Dorling, P. R. Fielden, S. W. Fogarty, N. J.  
121 Fullwood, K. A. Heys, C. Hughes, P. Lasch, P. L. Martin-Hirsch, B. Obinaju, G. D. Sockalingum, J. Sulé-Suso, R. J.  
122 Strong, M. J. Walsh, B. R. Wood, P. Gardner, and F. L. Martin, "Using Fourier transform IR spectroscopy to analyze  
123 biological materials," *Nat Protoc* **9**, 1771–1791 (2014).
- 124 2. T. W. Kee and M. T. Cicerone, "Simple approach to one-laser, broadband coherent anti-Stokes Raman scattering  
125 microscopy," *Opt. Lett.* **29**, 2701 (2004).
- 126 3. E. Ploetz, S. Laimgruber, S. Berner, W. Zinth, and P. Gilch, "Femtosecond stimulated Raman microscopy," *Appl.  
127 Phys. B* **87**, 389–393 (2007).
- 128 4. C. L. Evans, E. O. Potma, M. Puoris'haag, D. Côté, C. P. Lin, and X. S. Xie, "Chemical imaging of tissue *in vivo*  
129 with video-rate coherent anti-Stokes Raman scattering microscopy," *Proc. Natl. Acad. Sci. U.S.A.* **102**, 16807–16812  
130 (2005).
- 131 5. B. G. Saar, C. W. Freudiger, J. Reichman, C. M. Stanley, G. R. Holtom, and X. S. Xie, "Video-Rate Molecular  
132 Imaging In Vivo with Stimulated Raman Scattering," *Science* **330**, 1368–1370 (2010).
- 133 6. D. Fu, F.-K. Lu, X. Zhang, C. Freudiger, D. R. Pernik, G. Holtom, and X. S. Xie, "Quantitative Chemical Imaging  
134 with Multiplex Stimulated Raman Scattering Microscopy," *J. Am. Chem. Soc.* **134**, 3623–3626 (2012).
- 135 7. C.-S. Liao, M. N. Slipchenko, P. Wang, J. Li, S.-Y. Lee, R. A. Oglesbee, and J.-X. Cheng, "Microsecond scale  
136 vibrational spectroscopic imaging by multiplex stimulated Raman scattering microscopy," *Light Sci Appl* **4**, e265–e265  
137 (2015).
- 138 8. P. D. Chowdary, Z. Jiang, E. J. Chaney, W. A. Benalcazar, D. L. Marks, M. Gruebele, and S. A. Boppart, "Molecular  
139 Histopathology by Spectrally Reconstructed Nonlinear Interferometric Vibrational Imaging," *Cancer Res.* **70**,  
140 9562–9569 (2010).
- 141 9. Y. Ozeki, W. Umemura, Y. Otsuka, S. Satoh, H. Hashimoto, K. Sumimura, N. Nishizawa, K. Fukui, and K. Itoh,  
142 "High-speed molecular spectral imaging of tissue with stimulated Raman scattering," *Nat. Photon* **6**, 845–851 (2012).
- 143 10. D. Fu, G. Holtom, C. Freudiger, X. Zhang, and X. S. Xie, "Hyperspectral Imaging with Stimulated Raman Scattering  
144 by Chirped Femtosecond Lasers," *J. Phys. Chem. B* **117**, 4634–4640 (2013).
- 145 11. C. Di Napoli, I. Pope, F. Masia, P. Watson, W. Langbein, and P. Borri, "Hyperspectral and differential CARS  
146 microscopy for quantitative chemical imaging in human adipocytes," *Biomed. Opt. Express* **5**, 1378 (2014).

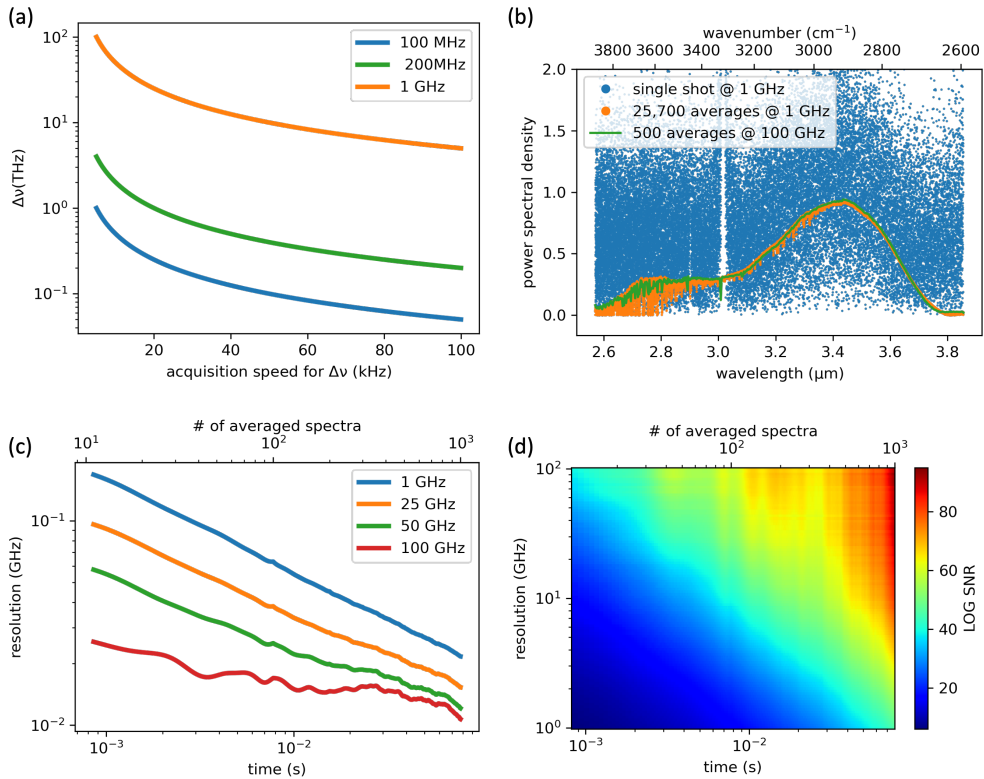


Fig. 6. Summary of DCS Imaging Speed. (a) The size of the optical Nyquist window plotted against acquisition speed ( $\Delta f_r$ ) for different repetition rates. (b) DCS spectrum taken at different averaging times and frequency resolution/apodization windows. (c) The spectra's SNR follow the scaling of Eq.2, with an example of the 2D parameter space (d) mapped out for the 1-GHz system.

- 147 12. H. Lin, H. J. Lee, N. Tague, J.-B. Lugagne, C. Zong, F. Deng, J. Shin, L. Tian, W. Wong, M. J. Dunlop, and J.-X.  
148 Cheng, "Microsecond fingerprint stimulated Raman spectroscopic imaging by ultrafast tuning and spatial-spectral  
149 learning," *Nat Commun* **12**, 3052 (2021).
- 150 13. T. Ideguchi, S. Holzner, B. Bernhardt, G. Guelachvili, N. Picqué, and T. W. Hänsch, "Coherent Raman spectro-imaging  
151 with laser frequency combs," *Nature* **502**, 355–358 (2013).
- 152 14. M. J. Nasse, M. J. Walsh, E. C. Mattson, R. Reininger, A. Kajdacsy-Balla, V. Macias, R. Bhargava, and C. J.  
153 Hirschmugl, "High-resolution Fourier-transform infrared chemical imaging with multiple synchrotron beams," *Nat Methods* **8**, 413–416 (2011).
- 155 15. F. Ullah Khan, G. Guarnizo, and P. Martín-Mateos, "Direct hyperspectral dual-comb gas imaging in the mid-infrared,"  
156 *Opt. Lett.* **45**, 5335 (2020).
- 157 16. M. Tamamitsu, Y. Sakaki, T. Nakamura, G. K. Podagatlapalli, T. Ideguchi, and K. Goda, "Ultrafast broadband  
158 Fourier-transform CARS spectroscopy at 50,000 spectra/s enabled by a scanning Fourier-domain delay line," *Vib.  
159 Spectrosc.* **91**, 163–169 (2017).
- 160 17. K. Yeh, S. Kenkel, J.-N. Liu, and R. Bhargava, "Fast Infrared Chemical Imaging with a Quantum Cascade Laser,"  
161 *Anal. Chem.* **87**, 485–493 (2015).
- 162 18. I. Coddington, N. Newbury, and W. Swann, "Dual-comb spectroscopy," *Optica* **3**, 414 (2016).
- 163 19. N. Hoghooghi, S. Xing, P. Chang, D. Lesko, A. Lind, G. Rieker, and S. Diddams, "Broadband 1-GHz mid-infrared  
164 frequency comb," *Light Sci Appl* **11**, 264 (2022).
- 165 20. N. B. Hébert, J. Genest, J.-D. Deschênes, H. Bergeron, G. Y. Chen, C. Khurmi, and D. G. Lancaster, "Self-corrected  
166 chip-based dual-comb spectrometer," *Opt. Express* **25**, 8168 (2017).
- 167 21. N. B. Hébert, V. Michaud-Belleau, J.-D. Deschênes, and J. Genest, "Self-Correction Limits in Dual-Comb  
168 Interferometry," *IEEE J. Quantum Electron.* **55**, 1–11 (2019).
- 169 22. N. R. Newbury, I. Coddington, and W. Swann, "Sensitivity of coherent dual-comb spectroscopy," *Opt. Express* **18**,

- 170 7929 (2010).
- 171 23. A. J. Lind, A. Kowligy, H. Timmers, F. C. Cruz, N. Nader, M. C. Silfies, T. K. Allison, and S. A. Diddams,  
172 “Mid-Infrared Frequency Comb Generation and Spectroscopy with Few-Cycle Pulses and  $\chi(2)$  Nonlinear Optics,”  
173 Phys. Rev. Lett. **124**, 133904 (2020).
- 174 24. H. Timmers, A. Kowlagy, A. Lind, F. C. Cruz, N. Nader, M. Silfies, G. Ycas, T. K. Allison, P. G. Schunemann, S. B.  
175 Papp, and S. A. Diddams, “Molecular fingerprinting with bright, broadband infrared frequency combs,” Optica **5**,  
176 727 (2018).
- 177 25. H. Timmers, A. Kowlagy, A. J. Lind, N. Nader, J. Shaw, D. Zalvidea, J. Biegert, and S. A. Diddams, “Hyperspectral  
178 Microscopy with Broadband Infrared Frequency Combs,” in *Conference on Lasers and Electro-Optics*, (OSA, San  
179 Jose, California, 2019), p. SF1E.4.